*Article*

# Synergistic Effect of Nanoclay and Barium Sulfate Fillers on the Corrosion Resistance of Polyester Powder Coatings

**Jinbao Huang** [1,2,3], **Marshall Shuai Yang** [3,4], **Chengqian Xian** [5], **James Joseph Noël** [4,6,*], **Yolanda Susanne Hedberg** [4,6,*], **Jian Chen** [4], **Ubong Eduok** [4], **Ivan Barker** [6], **Jeffrey Daniel Henderson** [6], **Haiping Zhang** [7], **Liqin Wang** [1,2,*], **Hui Zhang** [3,*] **and Jesse Zhu** [3]

1   School of Mechatronics Engineering, Harbin Institute of Technology, Harbin 150001, China; jinbao.huang@hit.edu.cn
2   Zhengzhou Research Institute, Harbin Institute of Technology, Zhengzhou 450000, China
3   Department of Chemical and Biochemical Engineering, Western University, London, ON N6A 5B9, Canada; marshall.yang@uwo.ca (M.S.Y.); jzhu@uwo.ca (J.Z.)
4   Department of Chemistry, Western University, London, ON N6A 5B7, Canada; jchen496@uwo.ca (J.C.); ueduok@uwo.ca (U.E.)
5   Department of Statistical and Actuarial Sciences, Western University, London, ON N6A 5B7, Canada; cxian3@uwo.ca
6   Surface Science Western, Western University, London, ON N6G 0J3, Canada; ivan.barker@uwo.ca (I.B.); jhende64@uwo.ca (J.D.H.)
7   School of Chemical Engineering and Technology, Tianjin University, Tianjin 300072, China; hpzhang@tju.edu.cn
*   Correspondence: jjnoel@uwo.ca (J.J.N.); yhedberg@uwo.ca (Y.S.H.); lqwang@hit.edu.cn (L.W.); hzhang1@uwo.ca (H.Z.); Tel.: +1-519-661-2111 (ext. 88029) (J.J.N. & Y.S.H.); +86-138-9575-5121 (L.W.); +1-519-661-2111 (ext. 81294) (H.Z.)

**Abstract:** Nanoclay has proven to be an active anti-corrosive additive due to the self-repairing effect from nanoclay swelling and expansion, except for its passive barrier effect due to the high aspect ratio. But it is still uncertain how these effects of nanoclay are intertwined with the other components in a complex coating system in corrosive environments. In this study, we examined the combined effects of nanoclays of two particle sizes with a commonly used cost-reducing filler, BaSO$_4$. By employing neutral salt spray tests, electrochemical analysis, and surface characterization, we identified the optimal conditions for achieving a strong barrier effect. Surprisingly, a relatively low nanoclay dosage of 2% combined with BaSO$_4$ filler exhibited synergistic behavior. Nanoclay not only compensated for the reduction in the barrier effect owing to the addition of BaSO$_4$ by offering self-repairing and barrier effects, but also overcame the delamination issues observed at higher nanoclay dosages (4% and above). The coating panel with 2% larger nanoclay and BaSO$_4$ showed two orders of magnitude higher pore resistance than the coating without nanoclay, remaining at $10^7$ $\Omega \cdot cm^2$ after 25 days of immersion. As a result, this coating panel demonstrated significantly slower corrosion expansion and reached a lifetime of 2500 h when creepage exceeded 2 mm in salt spray tests. This study contributes to a full understanding and proper utilization of nanoclay for high-performance, smart anti-corrosive coatings.

**Keywords:** montmorillonite; additive; anti-corrosive; powder paint; polyester/TGIC; extender; BaSO$_4$; barium sulphate; electrochemical impedance spectroscopy; EIS

## 1. Introduction

Anti-corrosive coatings are crucial in protecting metallic materials, making them economically and technically significant. Extensive research efforts have been devoted to understanding their protection mechanisms and enhancing their performance [1,2]. The corrosion process on uncoated or exposed steel substrates involves an electrochemical reaction, leading to material deterioration. Effective coatings with good substrate adhesion

serve as dense and compact barriers, reducing the permeability of aggressive ions such as $Cl^-$, oxygen and water, to the substrate. Such coatings can separate the anodic and cathodic regions, inhibit the cathodic half-reaction, and alleviate the burden of higher pH values that could degrade the coating binder [3,4]. Inadequate wet adhesion can also lead to coating delamination due to changes in internal stresses caused by water [5,6].

We have evaluated the performance of two commercially available montmorillonite-based nanoclays, Claytone® HT (C1) and CLOISITE® 30B (C2), as anti-corrosive additives in the polyester/triglycidyl isocyanurate (TGIC) clearcoat powder coating system [7]. Both clays have a layered structure and a high aspect ratio, which can increase the tortuosity of coating films, decrease the permeability, and slow down the electrolyte ingress when the coating is exposed to a corrosive environment [8,9]. Optimal dosages for each additive were determined through systematic incorporation into the coating binder, followed by evaluation using applicable ASTM standards, electrochemical measurements, and surface and structure characterization. The nanoclay with a larger particle size exhibited more superior barrier properties and self-repairing capabilities in the neutral salt spray and electrochemical tests than the smaller one [7].

In coating formulations, fillers or extenders are common additives alongside resin, curing agents, pigments, and other components [10,11]. Fillers contribute to reduced material costs and enhanced mechanical strength [3,12–14]. While talc and barium sulfate are known fillers for coatings, their combined use with other additives, such as montmorillonite, has demonstrated enhanced anti-corrosive performance [3,15–18]. When used alone in polyester/TGIC powder coatings, barium sulfate does not exhibit a barrier effect. Still, it can reduce the required dosage of zinc phosphate as an anti-corrosive pigment [15]. Moreover, montmorillonite has been shown to function as a dispersion aid for other polymer components [19].

Formulating coatings with multiple types of solid particles, including pigments, additives, and fillers, is common in research and industrial practices [20,21]. Such combinations are typically evaluated experimentally due to the complexity of interactions between the components. Studies on the combined effects are rare in the literature, and one of the objectives of this study is to explore this topic in volatile organic compound (VOC)-free powder coatings by electrochemical techniques.

This study further explores the incorporation of barium sulfate filler and the two nanoclays to reduce the cost of polyester/TGIC powder coatings. The corrosion resistance of the new coatings is investigated with electrochemical techniques in electrolyte immersion and neutral salt spray tests in salt fog. The mechanical performance and surface quality of coatings are crucial for industrial applications, and they are affected by the incorporation of additives and fillers. These properties need to be assessed and compared with the original coatings.

## 2. Experimental Section and Methods

### 2.1. Materials

The properties of the two nanoclay additives, Claytone® HT (C1) and CLOISITE® 30B (C2), with a chemical structure of $(Na,Ca)_{0.33}(Al,Mg)_2(Si_4O_{10})(OH)_2 \cdot nH_2O$ (BYK-Chemie GmbH, Wesel, Germany), are listed in Table 1. Both nanoclays are surface treated by quaternary ammonium salts, which provides organophilicity to the particles [22] and imrpoves the affinity between the clay and binder and enhancing particle dispersion [21]. To simulate a scenario closer to industrial practices, and to investigate the combined effect of the nanoclay additives with a filler, barium sulfate (Mountain Minerals, Calgary, AB, Canada, referred to as the "filler") was selected for its cost-effectiveness and widespread availability. The physical properties of the $BaSO_4$ are summarized in Table 2.

**Table 1.** The particle size distribution of the two nanoclays (measured with a laser particle size analyzer, BT9300S, Bettersize Instruments Ltd., Dandong, China).

| Symbol | Trade Name | Particle Size/μm | | | Density/(g/cm$^3$) |
|---|---|---|---|---|---|
| | | $D_{10}$, V | $D_{50}$, V | $D_{90}$, V | |
| C1 | Claytone$^®$ HT | 4.49 | 18.38 | 46.10 | 1.70 |
| C2 | CLOISITE$^®$ 30B | 1.91 | 8.64 | 23.08 | 1.98 |

**Table 2.** Physical properties of barium sulfate (BaSO$_4$, filler).

| Filler Name | Purity | Oil Absorption/(g/100 g) | Median Particle Diameter ($D_{50}$, V)/μm | Density/(g/cm$^3$) |
|---|---|---|---|---|
| Sparwite$^®$ W-10 | ≥97% | 10.00 | 2.10 | 4.40 |

The composition of the polyester/TGIC powder coatings is provided in Table 3. To investigate the combined effects of the two nanoclays, we formulated a series of coating samples with varying nanoclay dosages ranging from 2% to 16% (all percentages are mass fractions). The detailed formulations of these coatings are listed in Table 4. The filler was intentionally designed to constitute 15% of the remaining components in the coatings.

**Table 3.** Composition of polyester/TGIC powder coatings with filler (PB).

| Component | Composition | Content/wt.% |
|---|---|---|
| Resin | Carboxylated polyester | 90.30 |
| Curing Agent | TGIC | 6.80 |
| Flow and Leveling Agent | Polyacrylate | 1.60 |
| Degassing Agent | Benzoin | 0.80 |
| Pigment | Carbon black | 0.50 |

**Table 4.** Symbols and formulations of coatings with nanoclay (C1 or C2) and BaSO$_4$. The total weight for each formulation is 100 g.

| Symbol | Nanoclay/g | Filler/g | Binder/g |
|---|---|---|---|
| Control-PB | 0.00 | 15.00 | 85.00 |
| C1–02%-PB | 2.00 | 14.70 | 83.30 |
| C1–04%-PB | 4.00 | 14.40 | 81.60 |
| C1–06%-PB | 6.00 | 14.10 | 79.90 |
| C1–08%-PB | 8.00 | 13.80 | 78.20 |
| C1–16%-PB | 16.00 | 12.60 | 71.40 |
| C2–02%-PB | 2.00 | 14.70 | 83.30 |
| C2–04%-PB | 4.00 | 14.40 | 81.60 |
| C2–06%-PB | 6.00 | 14.10 | 79.90 |
| C2–08%-PB | 8.00 | 13.80 | 78.20 |
| C2–16%-PB | 16.00 | 12.60 | 71.40 |

## 2.2. Preparation of Powder Coating Panels

The manufacturing involved thorough pre-mixing and subsequent extrusion of all raw materials specified in the formulations. This process was carried out with a laboratory-scale extruder for powder coating (model SLJ-10, Donghui Powder Coating Equipment Co., Yantai, China). The temperature was kept at 80, 90, and 100 °C for the infeed, plastification, and homogenization zones. The screw feeder, twin-screw, and the rolling chiller were operated at a rotation speed of 10, 300 and 10 rpm, respectively. The resulting extrudates underwent a cooling process before being subjected to crushing, thereby producing chips that were subsequently pulverized. This pulverized material was sieved, yielding coating powders of about 35 μm median particle size ($D_{50}$, V).

The obtained coating powders were then sprayed onto standardized phosphated steel panels (76, 152 and 0.81 mm in width, length, and thickness, adhering to the ASTM D609 Type 2 standard [23]). The spraying was conducted with an electrostatic spraying gun (Gema Switzerland GmbH, St. Gallen, Switzerland) at a value of $-50$ kV in a spraying booth.

A curing schedule was administered to all powder-coated panels in an oven under 200 °C for 15 min. This process guaranteed the complete cross-linking and subsequent full curing of the binders. The film thickness was kept at $60 \pm 5$ μm, as measured with a thickness gauge (PosiTector 6000, DeFelsko Corporation, Ogdensburg, NY, USA), according to ASTM D7091-13 [24].

### 2.3. Characterization

To assess the electrochemical performances, the coated panels were subjected to open-circuit potential (OCP), linear polarization resistance (LPR), and electrochemical impedance spectroscopy (EIS) measurements with a Modulab XM Studio MTS ECS system (Solartron Analytical, AMETEK Scientific Instruments, Oak Ridge, TN, USA) (version 3.4) in a 5% NaCl solution. The LPR measurement was conducted within the range of $\pm 10$ mV based on a stable OCP at a 10 mV/min scan rate. The slope of the potential–current (E-I) curve in this pseudo-linear region was calculated as the $R_p$ (polarization resistance) value. The EIS was performed using an amplitude of 10 mV (absolute) in the 10 mHz to 100 kHz range. The coated panel was the working electrode, a saturated calomel electrode (SCE) was the reference, and a Pt foil was the counter electrode. These electrochemical measurements were conducted at one-day intervals and the EIS data were fitted with ZView version 4.0 h.

The surface and cross-section morphology was characterized with a Hitachi SU3500 variable pressure scanning electron microscope (SEM, Hitachi High-Technologies Corporation, Tokyo, Japan). The confocal laser scanning microscopy (CLSM) was performed with a Zeiss LSM800 for materials (Carl Zeiss Microscopy Deutschland GmbH, Oberkochen, Germany). The confocal datasets were processed with ConfoMap (Digital Surf, Besançon, France) version 7.4.8341. The salt spray tests were conducted with an MX-9204 salt fog chamber (Associated Environmental Systems, Acton, MA, USA).

The coating surface qualities were investigated by measuring the specular gloss and distinctness-of-image (DOI) with a Rhopoint IQ 20/60 gloss haze DOI meter (Rhopoint Instruments Ltd., St. Leonards-on-Sea, UK). Mechanical properties, including the adhesion by tape test, pencil hardness, and impact resistance, were measured with an Elcometer 107 cross-hatch cutter (Elcometer Limited, Manchester, UK), a BYK 5800 pencil hardness tester (BYK-Gardner GmbH, Geretsried, Germany), and an Elcometer 1615 variable impact tester (Elcometer Limited, Manchester, UK), respectively.

## 3. Results and Discussion

### 3.1. Morphologies and Properties

The cross-sections of the coating films with the filler are presented in Figure 1a–h. The filler particles were uniformly dispersed into the coating binder, with minimal agglomerates exceeding 10 μm in size. Proper dispersion of the clay particles within the binder matrices was observed at relatively low dosages, exhibiting a defect-free surface without any visible pores. However, the coatings failed to form a continuous film at C1 dosages of 8% and 16%, resulting in a sandpaper-like appearance. Large pores and channels up to 10 μm (Figure 1e,f) were formed inside the coating films. Comparing the same dosage of 2% with and without the filler, it was evident that the incorporation of the filler led to smaller particle sizes in the nanoclay, facilitating its improved dispersion. The filler particles served as an effective dispersing agent, breaking down nanoclay particle agglomerates.

The confocal maps (Figure 1i–k) demonstrated a noticeable increase in surface roughness with higher nanoclay content, with the arithmetic average surface roughness, Sa, increasing from 0.6 to 5.6 μm as nanoclay content increased to 4%. Moreover, after the

immersion test, localized delamination between the steel substrate and the coating film was observed (Figure 1l–n).
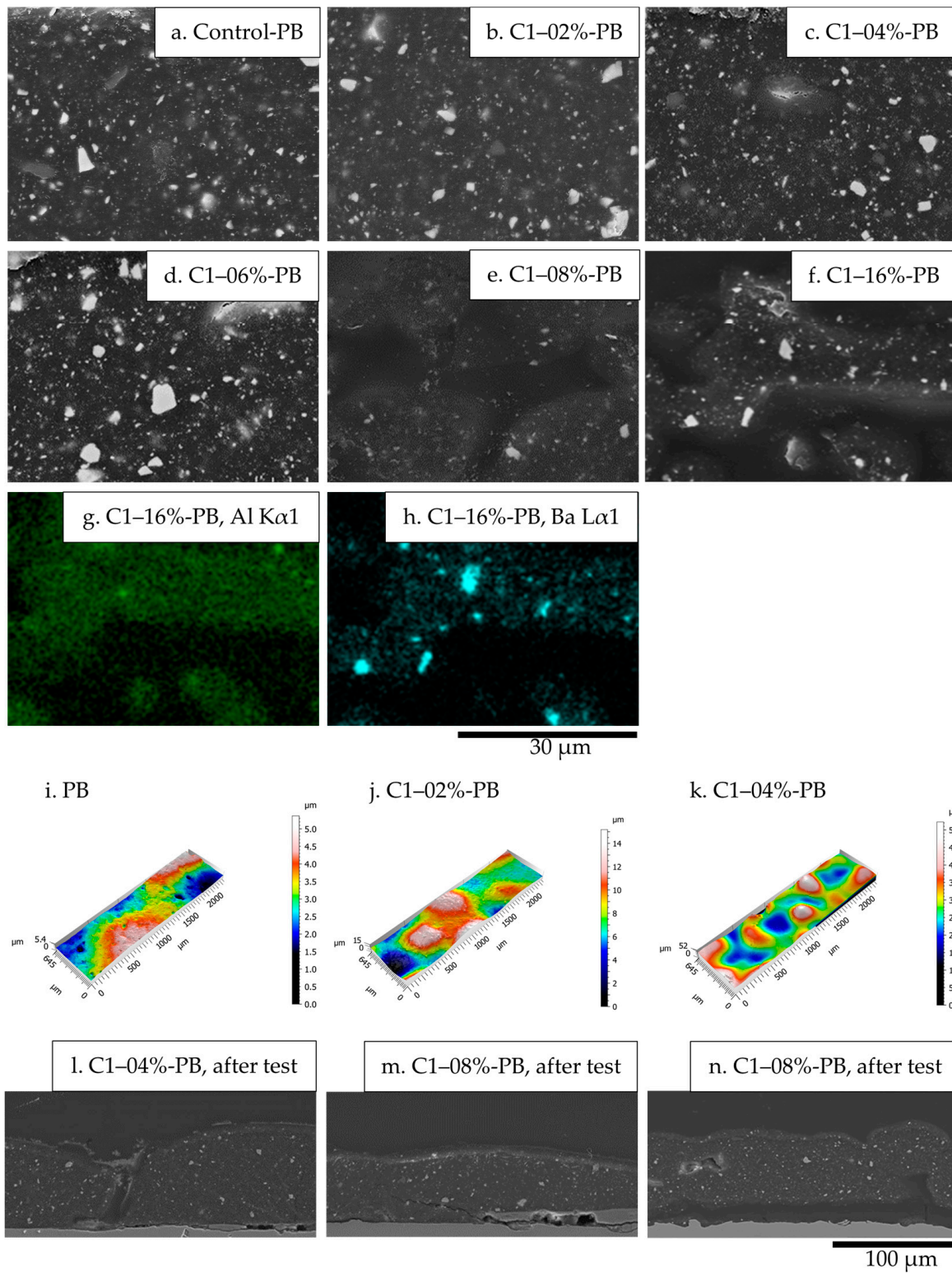


**Figure 1.** (**a**–**f**) SEM images, cross-sections of coatings with C1 dosages of 0–16%; (**g**,**h**) EDS maps of Al and Ba, coating with C1 16%; (**i**–**k**) confocal maps of coatings with C1. The Sa, for PB, C1–02%-PB, C1–04%-PB is 0.6 μm, 1.8 μm and 5.6 μm, respectively; (**l**–**n**) coatings with delaminated areas after immersion test, C1 4% and 8%.

Comparing the cross-section images of coatings with C2, as depicted in Figure 2a–f, it becomes evident that the nanoclay of a smaller particle size (C2) exhibited inferior dispersion within the coating matrix. At the dosage of 2%, the particles in Figure 2b (C2–02%-PB) are even larger in size compared to Figure 1b (C1–02%-PB), given that C2 has significantly smaller particles in its original powder form. This behavior is attributed to the stronger inter-particle forces experienced by smaller particles, leading to a higher tendency for agglomeration [25]. However, despite the less favorable dispersion, C2 had a less severe impact on the surface roughness, as demonstrated in Figure 2g–i. The Sa increased from 0.6 to 5.3 μm as the nanoclay content reaching 4 wt.%. However, an excessive nanoclay C2 content of 8% also led to inferior surface quality and defects inside the film, as shown in Figure 2j–l.
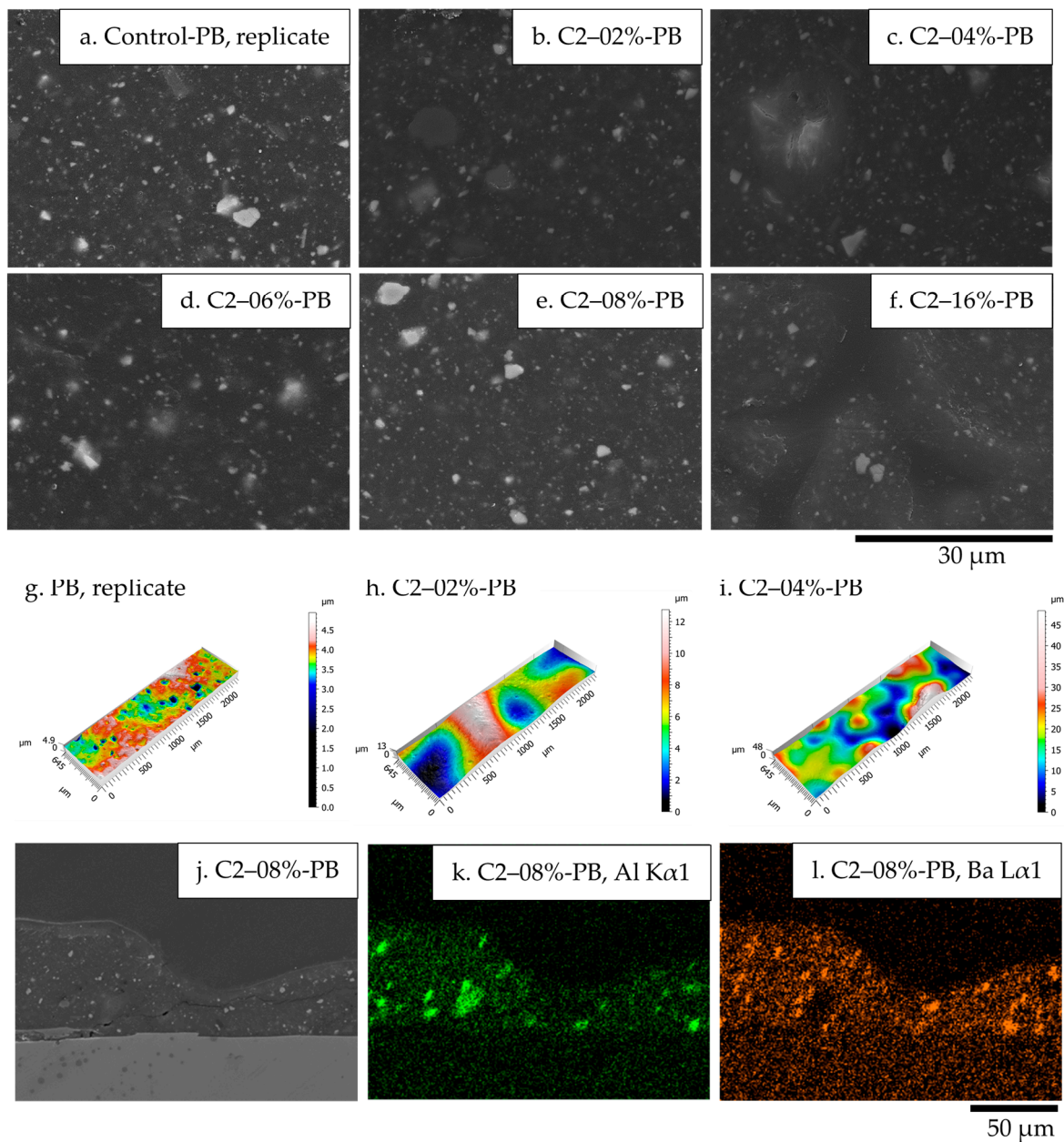


**Figure 2.** (**a**–**f**) SEM images, cross-sections of coatings with C2 dosages of 0–16%; (**g**–**i**) confocal maps of the coating with C2. The Sa, for PB, C2-02%-PB, C2-04%-PB is 0.6 μm, 1.7 μm and 5.3 μm, respectively; (**j**–**l**) SEM and EDS maps of Al and Ba, coating with C2 8%.

The surface quality of the coatings was studied based on their specular gloss [26] and distinctness-of-image (DOI) [27]. Figure 3 illustrates that both gloss and DOI declined with nanoclay dosage. Notably, the coatings containing nanoclay C2 displayed slightly higher surface quality than those with nanoclay C1, aligning with the observations from the confocal mapping, indicating a less severe impact on surface roughness for coatings with C2.
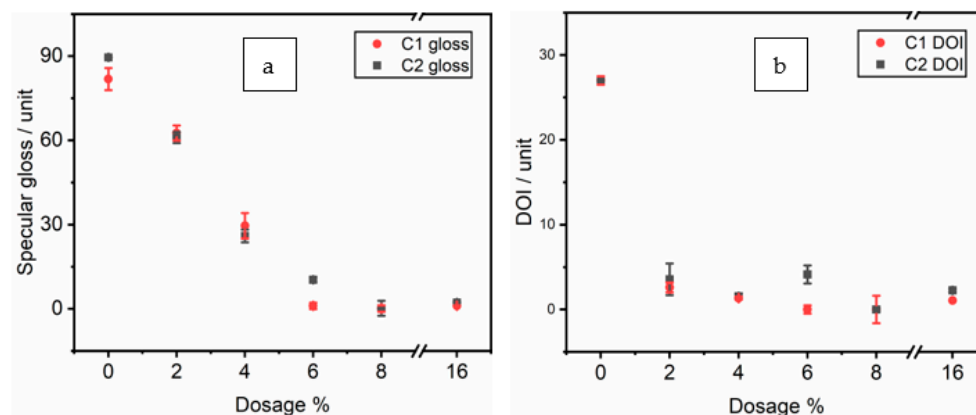


**Figure 3.** (**a**) specular gloss and (**b**) DOI of coatings with different contents of nanoclay.

Both series of coatings demonstrated good adhesion, achieving 4B as per ASTM D3359-09 [28], and exhibited the same pencil hardness of 2B as per ASTM D3363-05 [29]. The impact resistance values of the coatings, measured at 20 kg·cm, remained consistent with those obtained from the Control-PB formula, following the ASTM D2794-93 (Reapproved 2010) standard [30]. These results indicate that the incorporation of nanoclay and filler did not adversely influence the mechanical properties of the coatings.

Furthermore, despite adding nanoclay at a 4% dosage, the coatings maintained a desirable matte visual appearance, making them suitable for corrosion protection applications in the industry.

### 3.2. Electrochemical Measurements

#### 3.2.1. OCP and $R_p$ Measurement Results

The OCP and $R_p$ measurement results for the coatings containing the two nanoclays and the filler are depicted in Figure 4. Both series of coatings with 2% nanoclay showed the highest OCP (versus saturated calomel electrode (SCE)) and $R_p$ values over time [31]. The larger particle size exhibited superior performance, as evident from the $R_p$ values of $10^9$ and $10^7$ $\Omega \cdot cm^2$. During the immersion period, instances of $R_p$ increase were observed, indicating the self-repairing ability of the nanoclay.

Comparing these results with the $R_p$ values obtained for the optimal condition of C1 (4%) in the previous study (ranging between $10^9$ and $10^8$ $\Omega \cdot cm^2$) [7], it is evident that the current coatings, which include the $BaSO_4$, provided a slightly lower level of long-term barrier protection. However, this drawback is offset by the significant reduction in cost (about 15%). On the other hand, the addition of $BaSO_4$ alone cannot improve the barrier effect, as the presence of defects within the coating film outweighed any potential benefits in barrier properties [15].

Combining the two components (nanoclay and filler) in the coatings resulted in a balanced system that effectively controlled both the barrier properties and the formation of pores required to initiate nanoclay expansion.
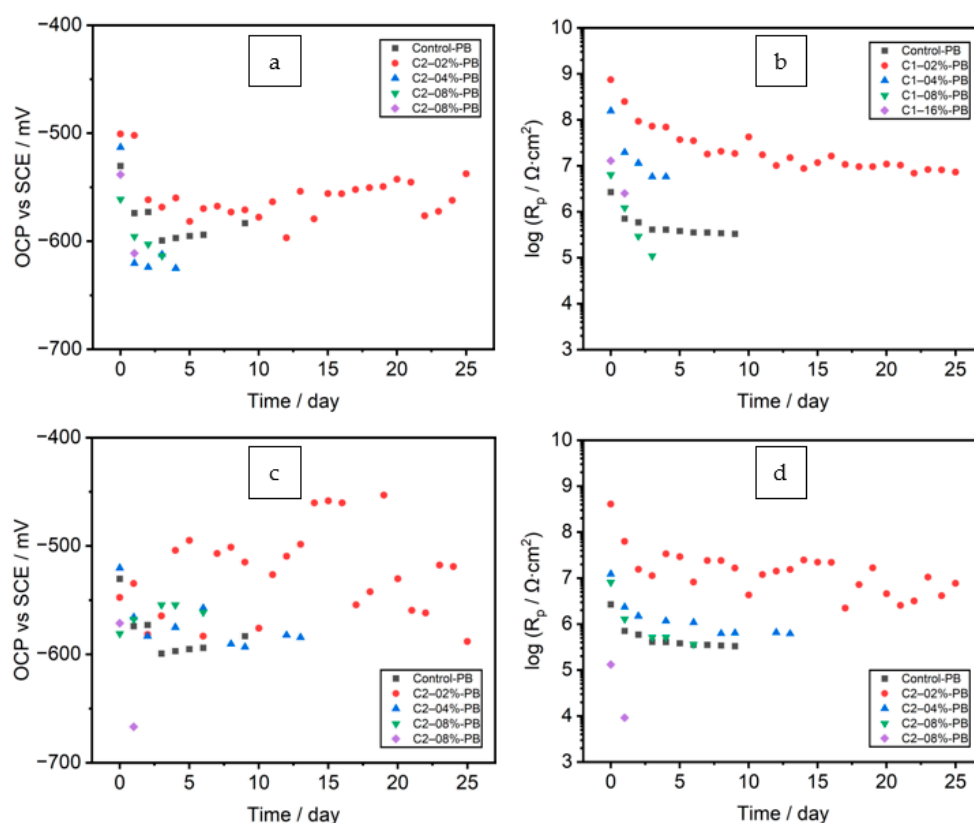
**Figure 4.** OCP and $R_p$ values for coatings with 0–16% C1 (**a**,**b**), and C2 (**c**,**d**).

### 3.2.2. Electrical Equivalent Circuit Analysis

Electrochemical impedance spectroscopy (EIS) measurements were conducted on the coatings C1–02%-PB and C2–02%-PB for 25 days when the sample showed about 0.03% rusted area, a rust grade of 9-G following the ASTM D610-08 standard [32].

The EIS data can be categorized into two groups based on the appearance of diffusional behavior observed on Day 4, as depicted in Figures 5 and 6. For Days 0–3, data fitting was performed with an equivalent electrical circuit (EEC) illustrated in Figure 5e. Subsequently, the EEC in Figure 6e, featuring Warburg element ($W_s$), was employed for data fitting from Day 4 onwards.

Figure 7 presents the fitted values of pore resistance ($R_{pore}$) for the two coatings C1–02%-PB, and C2–02%-PB. Comparative analysis reveals that the larger nanoclay provided a higher level of barrier enhancement. This can be attributed to the larger contact area of the coarser particles with the binder matrices. Additionally, the finer particles resulted in significantly more entrapped air packets on their surfaces, leading to aggravated electrolyte ingress [7]. Consequently, the coating with 4% nanoclay C1 exhibited the highest performance, as evidenced by its highest $R_{pore}$, aligning with the results from the OCP and $R_p$ measurements.

During the immersion period, an increase in the constant phase element ($CPE_{coat}$) and the corresponding exponential factor $\alpha_{coat}$ values of the coatings was observed for coatings C1–02%-PB and C2–02%-PB, indicating the self-repairing function of the nanoclay [7]. Additionally, a decrease in the charge transfer resistance ($R_{ct}$) value signified the delamination of the coating from the substrate [33,34], as shown in salt spray tests. The obtained values from the data fitting are listed in Tables 5 and 6; comparing the values, the coating with nanoclay C1 exhibited a higher performance, as shown by the lower double-layer capacitance CPE, similar $R_{pore}$, and higher charge transfer resistance values.
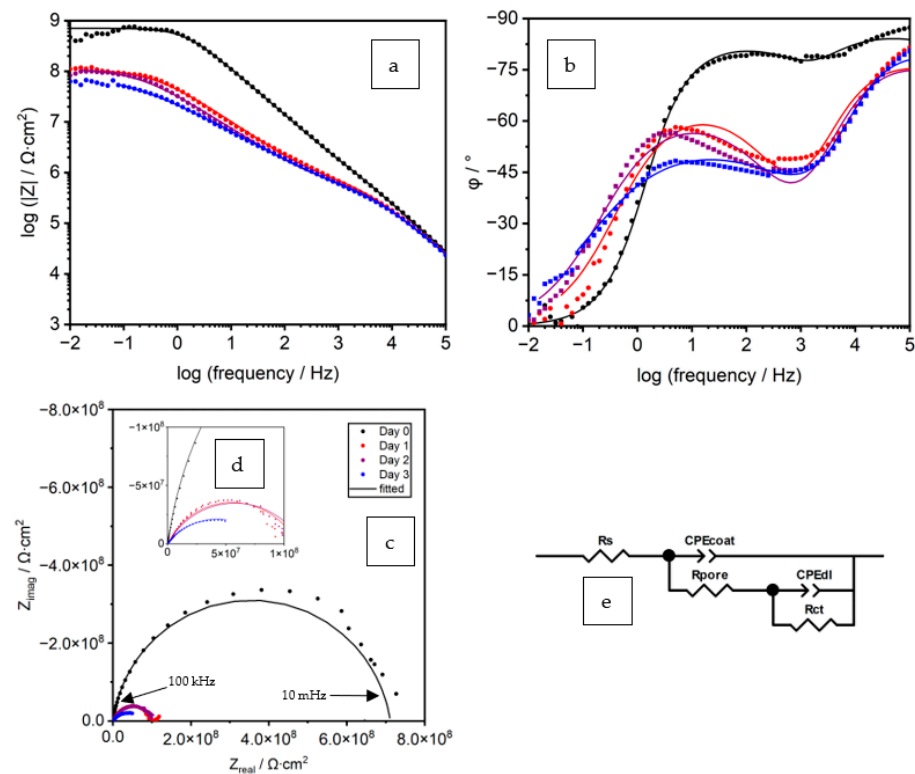
**Figure 5.** (**a**–**d**) Representative EIS spectra of the coated panel (C1–02%-PB) from day 0 to day 3, (**e**) the EEC used for fitting.
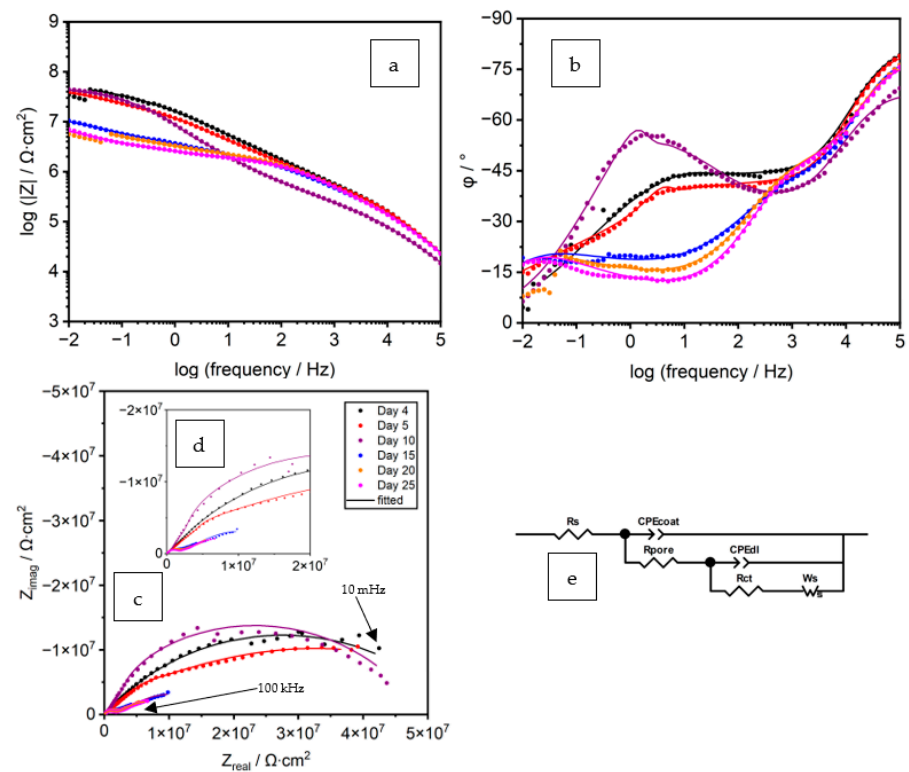


**Figure 6.** (**a**–**d**) Representative EIS spectra of coated panel C1–02%-PB, from day 4 to day 25, (**e**) the EEC used for fitting.
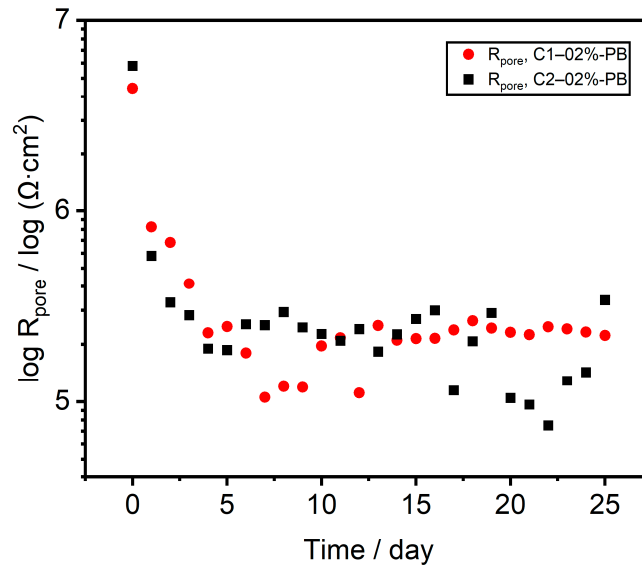
**Figure 7.** Comparison between the coatings with two nanoclays at 2% with filler and C1 at 2% without filler by fitted values of R$_{pore}$.

**Table 5.** Fitted values from the EEC analysis, a representative coating prepared from the formula C1–02%-PB.

| Time | CPE$_{coat}$ | | R$_{pore}$ | CPE$_{dl}$ | | R$_{ct}$ | W$_s$, R$_D$ | W$_s$, T$_D$ | W$_s$, P | $\chi^2$ |
|---|---|---|---|---|---|---|---|---|---|---|
| Days | $Q_c/$ $\Omega^{-1} \cdot cm^{-2} \cdot s^{\alpha}$ | $\alpha_{coat}$ | $\Omega \cdot cm^2$ | $Q_d/$ $\Omega^{-1} \cdot cm^{-2} \cdot s^{\alpha}$ | $\alpha_{dl}$ | $\Omega \cdot cm^2$ | $\Omega \cdot cm^2 \cdot s^P$ | S | | |
| 0 | $1.13 \times 10^{-10}$ | 0.949 | $4.43 \times 10^6$ | $8.17 \times 10^{-11}$ | 0.856 | $7.70 \times 10^8$ | | | | $6.32 \times 10^{-3}$ |
| 1 | $3.52 \times 10^{-10}$ | 0.870 | $8.23 \times 10^5$ | $4.42 \times 10^{-9}$ | 0.715 | $1.10 \times 10^8$ | | | | $3.17 \times 10^{-3}$ |
| 2 | $2.00 \times 10^{-10}$ | 0.868 | $6.81 \times 10^5$ | $7.18 \times 10^{-9}$ | 0.683 | $1.15 \times 10^8$ | | | | $2.48 \times 10^{-3}$ |
| 3 | $1.34 \times 10^{-10}$ | 0.916 | $4.14 \times 10^5$ | $1.13 \times 10^{-8}$ | 0.582 | $8.50 \times 10^7$ | | | | $4.52 \times 10^{-4}$ |
| 4 | $1.25 \times 10^{-10}$ | 0.951 | $2.29 \times 10^5$ | $1.85 \times 10^{-8}$ | 0.527 | $1.72 \times 10^7$ | $3.08 \times 10^7$ | $4.31 \times 10^0$ | 0.500 | $2.52 \times 10^{-4}$ |
| 5 | $1.56 \times 10^{-10}$ | 0.936 | $2.47 \times 10^5$ | $3.60 \times 10^{-8}$ | 0.382 | $3.05 \times 10^4$ | $6.56 \times 10^6$ | $2.16 \times 10^1$ | 0.626 | $2.25 \times 10^{-4}$ |
| 10 | $1.35 \times 10^{-9}$ | 0.807 | $1.96 \times 10^5$ | $2.58 \times 10^{-8}$ | 0.611 | $1.15 \times 10^6$ | $4.70 \times 10^6$ | $5.39 \times 10^1$ | 0.647 | $6.80 \times 10^{-4}$ |
| 15 | $1.85 \times 10^{-10}$ | 0.923 | $2.14 \times 10^5$ | $8.55 \times 10^{-9}$ | 0.624 | $1.31 \times 10^6$ | $1.52 \times 10^6$ | $1.35 \times 10^4$ | 0.281 | $2.19 \times 10^{-4}$ |
| 20 | $2.25 \times 10^{-10}$ | 0.909 | $2.31 \times 10^5$ | $4.69 \times 10^{-9}$ | 0.674 | $1.34 \times 10^6$ | $1.46 \times 10^6$ | $2.47 \times 10^4$ | 0.287 | $7.60 \times 10^{-5}$ |
| 25 | $2.29 \times 10^{-10}$ | 0.908 | $2.22 \times 10^5$ | $4.98 \times 10^{-9}$ | 0.667 | $1.37 \times 10^6$ | $8.30 \times 10^6$ | $9.88 \times 10^3$ | 0.321 | $2.85 \times 10^{-4}$ |

**Table 6.** Fitted values from the EEC analysis, a representative coating prepared from the formula C2–02%-PB.

| Time | CPE$_{coat}$ | | R$_{pore}$ | CPE$_{dl}$ | | R$_{ct}$ | W$_s$, R$_D$ | W$_s$, T$_D$ | W$_s$, P | $\chi^2$ |
|---|---|---|---|---|---|---|---|---|---|---|
| Days | $Q_c/$ $\Omega^{-1} \cdot cm^{-2} \cdot s^{\alpha}$ | $\alpha_{coat}$ | $\Omega \cdot cm^2$ | $Q_d/$ $\Omega^{-1} \cdot cm^{-2} \cdot s^{\alpha}$ | $\alpha_{dl}$ | $\Omega \cdot cm^2$ | $\Omega \cdot cm^2 \cdot s^P$ | S | | |
| 0 | $5.96 \times 10^{-9}$ | 0.968 | $5.79 \times 10^6$ | $3.70 \times 10^{-8}$ | 0.666 | $8.12 \times 10^8$ | | | | $8.89 \times 10^{-4}$ |
| 1 | $5.73 \times 10^{-8}$ | 0.815 | $5.80 \times 10^5$ | $9.39 \times 10^{-7}$ | 0.622 | $1.42 \times 10^8$ | | | | $4.70 \times 10^{-4}$ |
| 2 | $1.21 \times 10^{-7}$ | 0.766 | $3.29 \times 10^5$ | $4.46 \times 10^{-6}$ | 0.545 | $3.74 \times 10^7$ | | | | $6.47 \times 10^{-4}$ |
| 3 | $1.12 \times 10^{-7}$ | 0.772 | $2.83 \times 10^5$ | $6.97 \times 10^{-6}$ | 0.482 | $2.92 \times 10^7$ | | | | $3.53 \times 10^{-4}$ |
| 4 | $4.65 \times 10^{-8}$ | 0.837 | $1.90 \times 10^5$ | $4.83 \times 10^{-6}$ | 0.459 | $1.17 \times 10^7$ | $1.01 \times 10^8$ | $4.12 \times 10^3$ | 0.500 | $6.05 \times 10^{-5}$ |
| 5 | $4.86 \times 10^{-8}$ | 0.833 | $1.87 \times 10^5$ | $4.99 \times 10^{-6}$ | 0.458 | $9.92 \times 10^6$ | $8.10 \times 10^7$ | $4.09 \times 10^3$ | 0. 500 | $6.72 \times 10^{-5}$ |
| 10 | $2.03 \times 10^{-7}$ | 0.726 | $2.26 \times 10^5$ | $1.67 \times 10^{-5}$ | 0.453 | $6.74 \times 10^6$ | $1.61 \times 10^6$ | $1.83 \times 10^3$ | 0. 500 | $4.25 \times 10^{-4}$ |
| 15 | $1.30 \times 10^{-7}$ | 0.767 | $2.70 \times 10^5$ | $6.51 \times 10^{-6}$ | 0.458 | $2.52 \times 10^6$ | $7.14 \times 10^7$ | $5.54 \times 10^3$ | 0.644 | $6.90 \times 10^{-4}$ |
| 20 | $7.78 \times 10^{-8}$ | 0.800 | $1.04 \times 10^5$ | $1.66 \times 10^{-5}$ | 0.370 | $2.14 \times 10^6$ | $2.68 \times 10^7$ | $4.97 \times 10^3$ | 0.648 | $5.00 \times 10^{-4}$ |
| 25 | $2.19 \times 10^{-6}$ | 0.594 | $3.39 \times 10^5$ | $7.15 \times 10^{-6}$ | 0.546 | $7.35 \times 10^5$ | $1.79 \times 10^7$ | $1.83 \times 10^2$ | 0.548 | $3.44 \times 10^{-4}$ |

### 3.3. Neutral Salt Spray Results

The neutral salt spray test, conducted as per ASTM B117 [35] and D1654-08 (Reapproved 2016) [36], was performed on the coated panels with 0.5 mm scribes. Figure 8 presents the hours required for each coating to exceed a mean creepage (W$_c$) of 2 mm. 3 replicates were tested for each formulation, and the time for one of the three to reach

the creepage (the shortest time for one of three) was recorded as the test result. The panel images taken at the conclusion of the test are displayed in Figure 9.
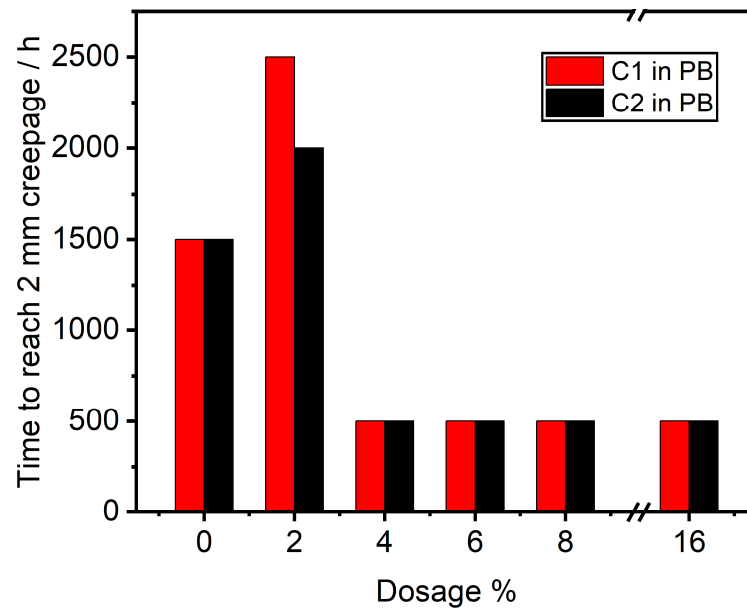


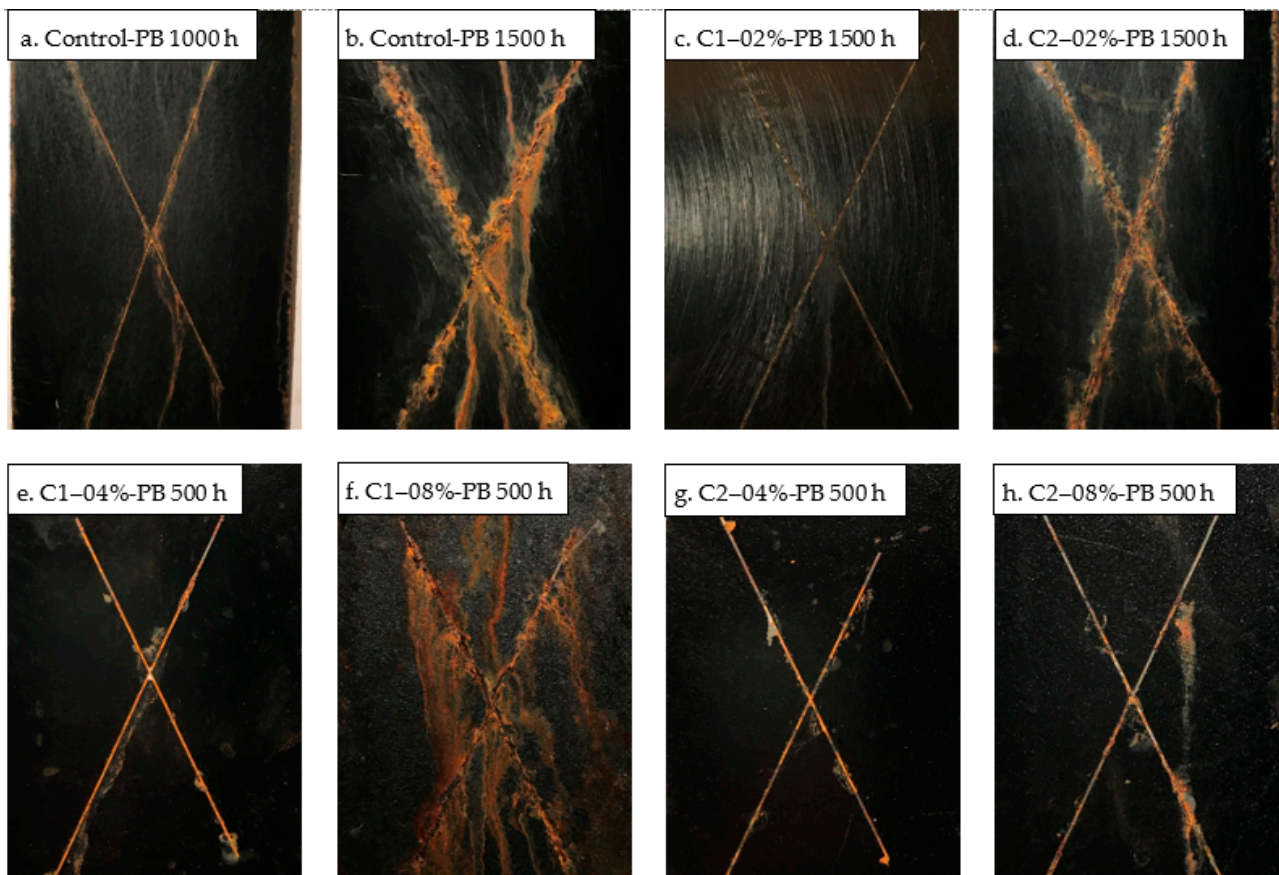**Figure 8.** Neutral salt spray results of the coatings incorporating nanoclays C1, C2 0–16% with the filler.



**Figure 9.** Representative coatings with nanoclays and the filler after neutral salt spray test, (**a**,**b**) PB-Control, (**c**,**d**) with C1, C2 2%, 1500 h, (**e**–**h**) with C1, C2, 4% and 8%, 500 h.

Among the coatings subjected to the same 2000 h salt spray duration, those containing the nanoclay with a larger particle size exhibited the highest level of anti-corrosive performance, with no apparent delamination observed along the scribe.

However, for coatings with nanoclay dosages starting from 4%, blisters formed along the scribe and adjacent coated areas [7]. This occurrence indicates a deterioration in the coating adhesion to the substrate, attributed to the swelling and expansion of the particles at higher contents. Such delamination became the primary cause of substrate corrosion propagation.

Remarkably, for coatings experiencing mechanical damage through scribing, the combination of a lower dosage of nanoclay and the filler demonstrated a significant synergistic effect. To avoid the detrimental impact of high nanoclay dosage, the optimal condition for nanoclay usage was the combination of 2% C1 with the filler. Comparatively, C2 of a smaller particle size led to more severe coating delamination, in agreement with its lower $R_{ct}$ values in Tables 5 and 6. This can be attributed to its larger number of particles and total surface area, leading to more pronounced swelling and expansion.

The results obtained from the electrochemical measurement on the original coatings and the neutral salt spray test on the scribed test panels correspond to different work conditions of the coatings, which are based on the risk of mechanical damage. In scenarios without the risk of mechanical damage, such as in storage tanks, the coatings with 4% nanoclay C1 without the filler exhibited the strongest barrier effect during immersion. However, for scenarios with the potential risk of mechanical damage, such as in a painted walkway, combining 2% nanoclay C1 with the filler in the coating proved to be a better choice. This combination showed significant synergistic effects, improving protective performance and resistance against delamination due to the mechanical damage caused by scribing, along with a reduction in coating cost and improved mechanical properties.

This discrepancy between the two test results agrees with our previous findings between anti-corrosive pigments, such as zinc phosphate, and the same filler, barium sulfate [15]. Future studies can further optimize the filler dosage to maximize the synergy between the two.

### 3.4. Conclusions

This study explored the incorporation of two nanoclays of different particle sizes into a UV-resistant polyester/TGIC powder coating system to enhance its anti-corrosive properties. Electrochemical and neutral salt spray tests were conducted to compare the performance of the coatings. The findings revealed that $BaSO_4$ can effectively decrease coating cost, but will inevitably decrease the barrier effect. A relatively low amount of 2% nanoclay can compensate for the reduction in the barrier effect by offering self-repairing and passive barrier effects and overcoming the delamination issues observed at higher nanoclay dosages (4% and above). The coating panel with 2% larger nanoclay and $BaSO_4$ showed 2 orders of magnitude higher pore resistance than the coating without nanoclay, remaining $10^7$ $\Omega \cdot cm^2$ after 25 days of immersion due to improved dispersion with the aid of the filler. As a result, this coating panel demonstrated significantly slow corrosion expansion and reached a lifetime of 2500 h when creepage exceeded 2 mm in salt fog tests. This study contributes to a better understanding the interaction between nanoclay and fillers in high-performance smart anti-corrosive coatings. It offers insights for formulating coatings suitable for different application scenarios.

**Author Contributions:** Methodology, J.H., M.S.Y., J.J.N., H.Z. (Hui Zhang) and I.B.; Validation, J.C., C.X. and U.E.; Investigation, J.H., H.Z. (Haiping Zhang) and J.D.H.; Resources, J.C., J.J.N., J.Z., L.W. and U.E.; Writing—original draft, J.H. and M.S.Y.; Writing—review & editing, M.S.Y., J.H., H.Z. (Haiping Zhang), H.Z. (Hui Zhang), J.C., Y.S.H., J.J.N., I.B., J.D.H., L.W. and C.X.; Visualization, J.J.N., U.E. and C.X.; Supervision, L.W., J.J.N., H.Z. (Hui Zhang) and Y.S.H.; Project administration, Y.S.H., H.Z. (Haiping Zhang) and J.Z.; Funding acquisition, H.Z. (Hui Zhang), L.W., J.J.N. and Y.S.H. All authors have read and agreed to the published version of the manuscript.

# References

1. Sørensen, P.A.; Kiil, S.; Dam-Johansen, K.; Weinell, C.E. Anticorrosive Coatings: A Review. *J. Coat. Technol. Res.* **2009**, *6*, 135–176. [CrossRef]
2. Montemor, M.F. Functional and Smart Coatings for Corrosion Protection: A Review of Recent Advances. *Surf. Coat. Technol.* **2014**, *258*, 17–37. [CrossRef]
3. Kalendova, A.; Veselý, D.; Kalenda, P. A Study of the Effects of Pigments and Fillers on the Properties of Anticorrosive Paints. *Pigment. Resin Technol.* **2006**, *35*, 83–94. [CrossRef]
4. Abdel-Gaber, A.M.; El Nabey, B.A.A.; Khamis, E.; Abdelattef, O.A.; Aglan, H.; Ludwick, A. Influence of Natural Inhibitor, Pigment and Extender on Corrosion of Polymer Coated Steel. *Prog. Org. Coat.* **2010**, *69*, 402–409. [CrossRef]
5. Sangaj, N.S.; Malshe, V.C. Permeability of Polymers in Protective Organic Coatings. *Prog. Org. Coat.* **2004**, *50*, 28–39. [CrossRef]
6. Negele, O.; Funke, W. Internal Stress and Wet Adhesion of Organic Coatings. *Prog. Org. Coat.* **1996**, *28*, 285–289. [CrossRef]
7. Yang, M.S.; Huang, J.; Zhang, H.; Noël, J.J.; Hedberg, Y.S.; Chen, J.; Eduok, U.; Barker, I.; Henderson, J.D.; Xian, C.; et al. Study on the Self-Repairing Effect of Nanoclay in Powder Coatings for Corrosion Protection. *Coatings* **2023**, *13*, 1220. [CrossRef]
8. Kotal, M.; Bhowmick, A.K. Polymer Nanocomposites from Modified Clays: Recent Advances and Challenges. *Prog. Polym. Sci.* **2015**, *51*, 127–187. [CrossRef]
9. Al-Shahrani, A.; Taie, I.; Fihri, A.; Alabedi, G. Polymer-Clay Nanocomposites for Corrosion Protection. In *Current Topics in the Utilization of Clay in Industrial and Medical Applications*; IntechOpen: London, UK, 2018. [CrossRef]
10. Spyrou, E. *Powder Coatings: Chemistry and Technology*, 3rd ed.; Vincentz Network GmbH & Co KG: Hannover, Germany, 2012; ISBN 978-3-86630-824-4.
11. Fu, J.; Krantz, M.; Zhang, H.; Zhu, J.; Kuo, H.; Wang, Y.M.; Lis, K. Investigation of the Recyclability of Powder Coatings. *Powder Technol.* **2011**, *211*, 38–45. [CrossRef]
12. Perera, D.Y. Effect of Pigmentation on Organic Coating Characteristics. *Prog. Org. Coat.* **2004**, *50*, 247–262. [CrossRef]
13. Li, W.; Franco, D.C.; Yang, M.S.; Zhu, X.; Zhang, H.; Shao, Y.; Zhang, H.; Zhu, J. Comparative Study of the Performances of $Al(OH)_3$ and $BaSO_4$ in Ultrafine Powder Coatings. *Processes* **2019**, *7*, 316. [CrossRef]
14. Fan, X. Mechanics of Moisture for Polymers: Fundamental Concepts and Model Study. In Proceedings of the EuroSimE 2008—International Conference on Thermal, Mechanical and Multi-Physics Simulation and Experiments in Microelectronics and Micro-Systems 2008, Breisgau, Germany, 20–23 April 2008; pp. 1–14. [CrossRef]
15. Yang, S.; Huang, J.; Chen, J.; Noël, J.J.; Barker, I.; Henderson, J.D.; He, P.; Zhang, H.; Zhang, H.; Zhu, J. A Comparative Study on the Anti-Corrosive Performance of Zinc Phosphate in Powder Coatings. *Coatings* **2022**, *12*, 217. [CrossRef]
16. Raju, A.; Lakshmi, V.; Vishnu Prataap, R.K.; Resmi, V.G.; Rajan, T.P.D.; Pavithran, C.; Prasad, V.S.; Mohan, S. Adduct Modified Nano-Clay Mineral Dispersed Polystyrene Nanocomposites as Advanced Corrosion Resistance Coatings for Aluminum Alloys. *Appl. Clay Sci.* **2016**, *126*, 81–88. [CrossRef]
17. Baby Suneetha, R.R.; Kulandaivel, S.; Vedhi, C. Synthesis, Characterisation and Electrochemical Application of Hybrid Nanocomposites of Polyaniline with Novel Clay Mineral. In *Materials Today: Proceedings*; Elsevier Ltd.: Amsterdam, The Netherlands, 2019; Volume 48, pp. 294–303.
18. Shirehjini, F.T.; Danaee, I.; Eskandari, H.; Zarei, D. Effect of Nano Clay on Corrosion Protection of Zinc-Rich Epoxy Coatings on Steel 37. *J. Mater. Sci. Technol.* **2016**, *32*, 1152–1160. [CrossRef]
19. Bouakaz, B.S.; Pillin, I.; Habi, A.; Grohens, Y. Synergy between Fillers in Organomontmorillonite/Graphene-PLA Nanocomposites. *Appl. Clay Sci.* **2015**, *116–117*, 69–77. [CrossRef]
20. Crapper, G. Powder Coatings. In *Polymer Science: A Comprehensive Reference*; Elsevier: Amsterdam, The Netherlands, 2012; Volume 10, pp. 541–566. ISBN 9780080878621.

21. Uddin, F. Montmorillonite: An Introduction to Properties and Utilization. In *Current Topics in the Utilization of Clay in Industrial and Medical Applications*; Zoveidavianpoor, M., Ed.; IntechOpen: London, UK, 2018; Volume i, pp. 1–23.

22. Guo, F.; Aryana, S.; Han, Y.; Jiao, Y. A Review of the Synthesis and Applications of Polymer-Nanoclay Composites. *Appl. Sci.* **2018**, *8*, 1696. [CrossRef]

23. *ASTM D609*; Standard Practice for Preparation of Cold-Rolled Steel Panels for Testing Paint, Varnish, Conversion Coatings, and Related Coating Products. ASTM International: West Conshohocken, PA, USA, 2017; pp. 1–3.

24. *ASTM D7091*; Standard Practice for Nondestructive Measurement of Dry Film Thickness of Nonmagnetic Coatings Applied to Ferrous Metals and Nonmagnetic, Nonconductive Coatings Applied to Non-Ferrous Metals. ASTM International: West Conshohocken, PA, USA, 2013; pp. 1–7.

25. Zhu, J.; Zhang, H. Ultrafine Powder Coatings: An Innovation. *Powder Coat.* **2005**, *16*, 39–47.

26. *ASTM D523*; Standard Test Method for Specular Gloss. ASTM International: West Conshohocken, PA, USA, 2014; pp. 1–5.

27. *ASTM D5767*; Standard Test Method for Instrumental Measurement of Distinctness-of-Image (DOI) Gloss of Coated Surfaces. ASTM International: West Conshohocken, PA, USA, 2018; pp. 1–7.

28. *ASTM D3359*; Standard Test Methods for Measuring Adhesion by Tape Test. ASTM International: West Conshohocken, PA, USA, 2009; pp. 1–8.

29. *ASTM D3363*; Standard Test Method for Film Hardness by Pencil Test. ASTM International: West Conshohocken, PA, USA, 2005.

30. *ASTM D2794*; Standard Test Method for Resistance of Organic Coatings to the Effects of Rapid Deformation (Impact). ASTM International: West Conshohocken, PA, USA, 1993.

31. Walter, G.W. A Critical Review of d.c. Electrochemical Tests for Painted Metals. *Corros. Sci.* **1986**, *26*, 39–47. [CrossRef]

32. *ASTM D610*; Standard Practice for Evaluating Degree of Rusting on Painted Steel Surfaces. ASTM International: West Conshohocken, PA, USA, 2008; pp. 1–6.

33. Loveday, D.; Peterspm, P.; Rodgers, B. Evalution of Organic Coatings with Electrochemical Impedance Spectroscopy Part 2: Application of EIS to Coatings. *Coat. Tech.* **2004**, *1*, 88–93.

34. Margarit-Mattos, I.C.P. EIS and Organic Coatings Performance: Revisiting Some Key Points. *Electrochim. Acta* **2020**, *354*, 136725. [CrossRef]

35. *ASTM B117*; Standard Practice for Operating Salt Spray (Fog) Apparatus. ASTM International: West Conshohocken, PA, USA, 2016.

36. *ASTM D1654*; Standard Test Method for Evaluation of Painted or Coated Specimens Subjected to Corrosive Environments. ASTM International: West Conshohocken, PA, USA, 2008; pp. 1–4.